FERMILAB-FN-0724 September 2002

Further Studies on Protecting LHC Components Against Radiation Resulting from an Unsynchronized Beam Abort

I.L. Rakhno, A.I. Drozhdin, N.V. Mokhov

Fermilab, P.O. Box 500, Batavia, IL 60510, USA

B. Goddard, M. Gyr, M. Sans, E. Weisse

CERN, Geneva, CH-1211, Switzerland

August 22, 2002

Abstract

The effect of possible accidental beam loss in the LHC on the IP5 and IP6 insertion elements is studied via realistic Monte Carlo simulations. The scenario studied is beam loss due to unsynchronized abort at an accidental prefire of one of the abort kicker modules. Simulations show that this beam loss would result in severe heating of the IP5 and IP6 superconducting (SC) quadrupoles. Contrary to the previous considerations with a stationary set of collimators in IP5, collimators in IP6 close to the cause are proposed: a movable collimator upstream of the Q4 quadrupole and a stationary one upstream of the extraction septum MSD. The calculated temperature rise in the optimal set of collimators is quite acceptable. All SC magnets are protected by these collimators against damage.

1 Introduction

An accidental beam loss caused by an unsynchronized abort launched at abort system malfunction, can cause severe damage to the collider equipment. Such a malfunction can be initiated, *e.g.*, by a spontaneous high voltage discharge in a kicker generator module or high energy cosmic particle crossing a sensitive element of the abort system trigger. A single prefired kicker module induces coherent beam oscillations with an amplitude up to 21σ of the beam at collision. Simulations show that if this happens at the top energy, starting from 70-80% of the kicker strength, the misbehaved beam ends up in the IP5 inner triplet causing destruction of its components [1]. To avoid this, the other kicker modules are fired immediately after (producing a full, unsynchronized, abort), but this does not prevent beam loss completely. At normal operation the kicker front is placed in a longitudinal gap in the circulating beam to prevent particle loss during the kicker pulse rise time. At the unsynchronized abort the kicker front does not coincide with this gap. As a result, it causes beam loss at the collider limiting aperture. A set of stationary shadow collimators for the IP5 has been proposed in [1] to protect its inner triplet against irreversible consequences of fast beam loss. Alternatively, an additional movable collimator TCDQ, in IP6 as close to the cause as possible, has been proposed in [2] to protect the entire LHC machine.

2 The Model Update

Results of previous calculations on protecting LHC components against radiation resulting from an unsynchronized beam abort were described in [2]. Since then, the dimensions of the graphite collimator TCDS (designed to protect the extraction septum) and the alignment of the extraction septum magnets MSD were changed at CERN in accordance with the latest updates of the LHC beam optics (version 6.2). The aim was to reduce further the energy deposition and temperature rise in the magnets MSD and downstream superconducting (SC) magnets. The present note describes the recent results obtained with the MARS14 code [3] and some comparisons with calculations by FLUKA [4]. A central part of the IP6 MARS calculation model and cross section of the 5-m long graphite collimator TCDS placed in front of the MSD modules are shown in Fig. 1.

The most significant update to the collimator is increase of its width from 20 to 23 mm. The updated configuration of the magnets MSD and its implementation in the MARS model are presented in Fig. 2. The most important update to the MSD magnets consists of shift of the modules in the outward direction. It results in better protection of the modules. The 9.5-m long graphite and aluminum collimator TCDQ is placed at a radial position of 9.1 mm, corresponding to $8\sigma_x$ of the circulating beam at collison energy of 7 TeV, plus orbit deviations.

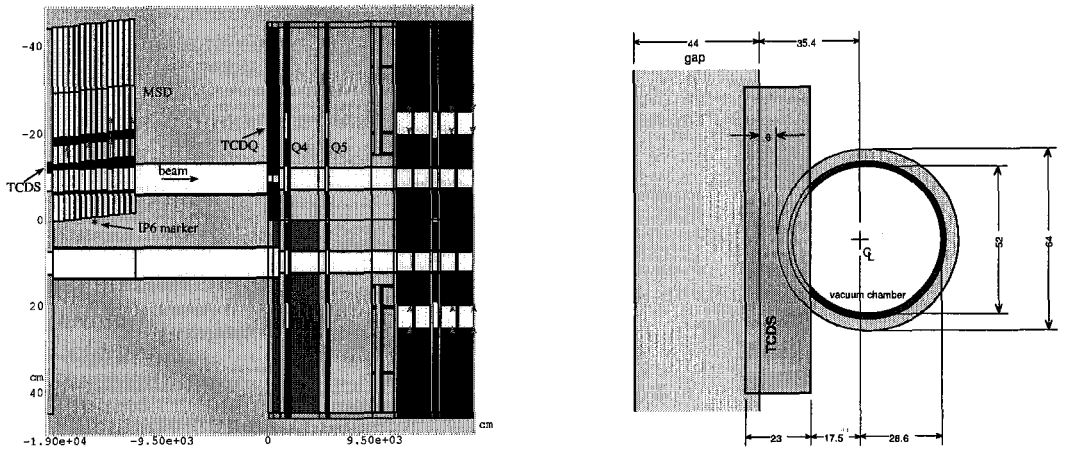

Figure 1: Central part of the IP6 MARS mode (left) and graphite collimator TCDS ($\rho = 1.77$ g/cm^3) to protect extraction septum magnets MSD (all dimensions are in mm) (right).

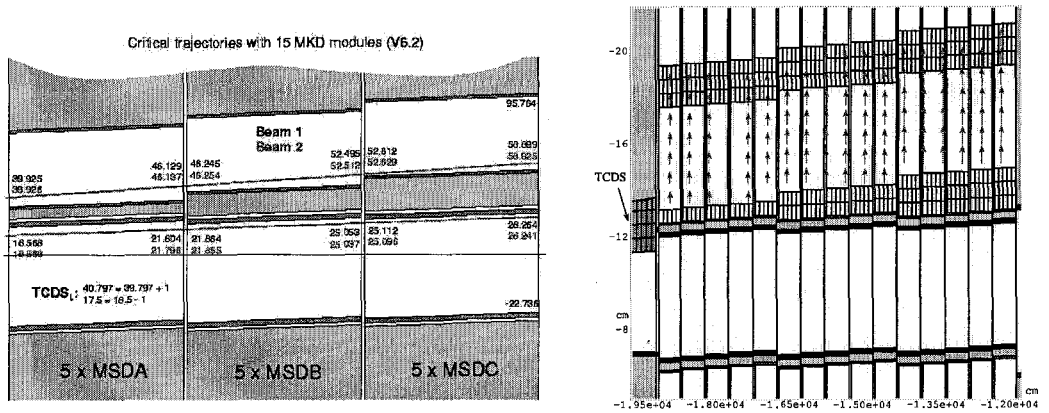

Figure 2: Extraction septum magnets MSD according to optimization optics studies at CERN (left) and MARS model for the magnets (right).

3 Beam Parameters

The beam characteristics used are described in Table 1. In our calculations, we assume that bunches are distributed uniformly along the accelerator and there is only one 3 μs abort gap in the circulating beam. To cover the abort kicker rise time of 3 μs (see Table 1), 280 bunches are considered which correspond to 7 μs. It enables us to investigate effect of delay time τ, *i.e.* time elapsed between prefiring the single kicker and firing the other ones. Results presented below were obtained for a kicker strength $B{\cdot}l = 63.05$ kG·m, which corresponds to an angle $\alpha = 0.27$ mrad at 7 TeV.

Table 1: LHC beam parameters used in calculations.

Proton energy	7000 GeV
Normalized transverse emittance (σ)	3.75 mm·mrad
Protons per bunch	$1.05 \cdot 10^{11}$
Number of bunches	2835
Total intensity	$3 \cdot 10^{14}$
Revolution time	88.924 μs
Horizontal crossing angle in the IP5	150 μrad
Horizontal closed orbit deviation	4 mm
Vertical closed orbit deviation	4 mm
Magnet misalignment	1 mm
Mechanical error	0.6 mm
Bunch separation (10 RF buckets)	24.95 ns
Abort gap (127 missing bunches)	3.17 μs
Number of abort kicker modules	14
Abort kicker rise time	3 μs

4 Heat Load

Calculated at the baseline luminosity two-dimensional distribution of incoming energy flux over cross section of the TCDS collimator (see Fig. 1) during an unsynchronized beam abort is presented in Fig. 3. Horizontal coordinate $y = 0$ (MARS notations) corresponds to the right edge of the collimator. During such an abort with the 1.2 μs delay, about 6.1 MJ of energy enters the TCDS collimator. The quantity amounts approximately to 1.7% of energy contained in the LHC beam.

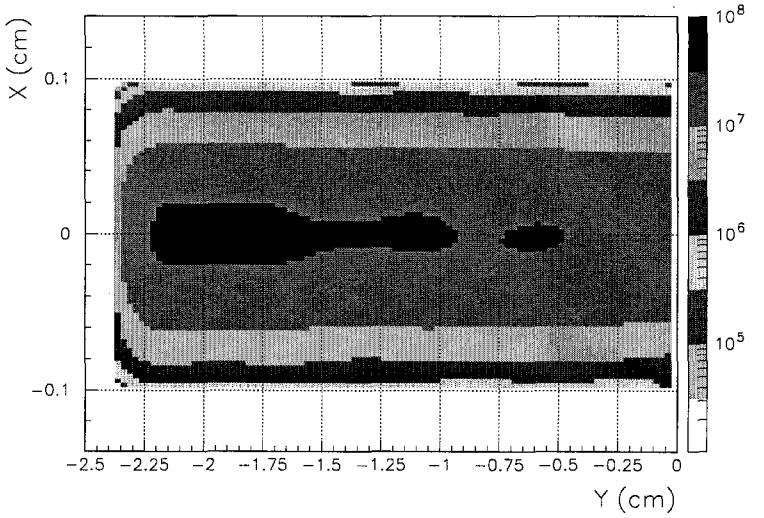

Figure 3: Energy flux isocontours (J/cm^2) at TCDS during an unsynchronized beam abort with τ=1.2 μs.

Table 2 gives total energy deposition in the collimators, MSD modules, and several SC magnets downstream of the IP6 marker. For the SC magnets, heat load includes energy deposited in the coils, beam screens, coolant (He) *etc.* up to, but not including, the steel vessel which separates the cold mass from the warm surroundings. Calculated statistical uncertainty for the first two rows in the Table does not exceed 5% and gradually increases up to 20% obtained for the last row. When comparing the previous data on integral energy deposition [2] with present data of Table 2, one can see that relative increase in energy deposited in the TCDS collimator is almost the same as relative increase in its width, i.e. about 15%. For the first of the MSD modules the relative increase is about 3-6% for all the delay times considered. Starting from the second module, for each of the subsequent ones downstream, the deposited energy in the present design is lower compared to the previous values [2]. At the same time, there were no changes in the model for the region downstream of TCDQ collimator; only small changes are observed in deposited energy in that region. Thus, one can state that the present design ensures better protection of the extraction modules and the SC magnets of the IP6 region.

Table 2: Heat load (kJ) in IP6 components.

Module	Relative position* (m)	Delay time τ (μs)		
		1.2	3.0	4.0
TCDS	-42.1	1120	1160	1150
MSD-1	-36.6	1340	1380	1380
MSD-6	-12.05	20	20	20
MSD-11	12.5	8	8	6
MSD-15	32.14	3	3	3
TCDQ-1	155.3	1640	2530	3470
TCDQ-2	159.3	528	1020	1630
TCDQ-3	160.8	60	149	299
Q4	170.1	22	86	235
Q5	206.5	4.6	23	68
MBA-1	270.1	3.0	16	45
MBB-1	285.8	0.64	3.6	10
Q8	302.1	0.11	0.27	0.9
MBA-2	309.2	0.30	0.61	2.5
MBB-2	324.8	0.17	0.55	1.7

*) Between upstream end and IP6 marker.

5 Temperature Rise

It has been found in [5] that calculated peak temperature rise distributions are insensitive to cell linear size at sizes less than $\frac{1}{2}\sigma$, where σ is RMS beam spot size of Gaussian profile (the rule applies to each of the two coordinates in a plane orthogonal to the beam). To get the distributions in the graphite collimator TCDQ, the cell size (hereinafter $\Delta x \Delta y \Delta z^*$) of $0.5\times11\times500$ mm^3 was chosen previously according to the rule [5]. For the graphite collimator TCDS and MSD modules additional calculations were performed for different cell sizes to determine the optimal ones. Initial temperature assumed is 27°C. The following conclusions can be made from the results presented in Fig. 4: (i) for the collimator TCDS the adequate cell size is $1\times6\times200$ mm^3; (ii) for a MSD module, smaller cells should be considered ($1\times1\times200$ mm^3) which reflects higher spatial energy deposition density in iron due to higher material density and atomic number compared to graphite. The empirically determined cell size along X-axis (1 mm) is in accordance with the rule [5].

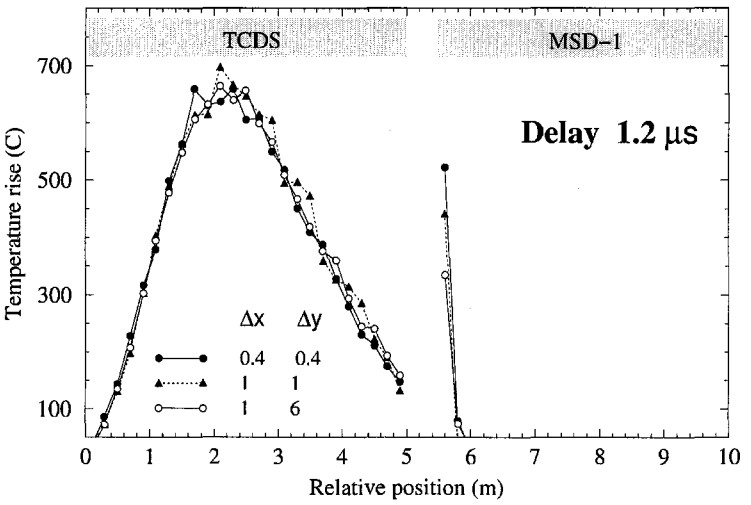

Figure 4: Peak temperature rise distributions along the hottest regions of the TCDS collimator and MSD-1 module calculated with several cell sizes Δx and Δy (in *mm*).

At the same time, distribution of the incident beam along Y-axis on the upstream face of the TCDS is almost uniform, so that the empirically determined cell size along Y-axis is preferable from the practical standpoint. Calculations with shorter cells (100 instead of 200 mm along Z-axis) revealed negligible changes in peak temperature rise distributions for the TCDS collimator, while for a MSD module the cell size $1\times1\times100$ mm^3 is more adequate. According to the MARS calculations, the hottest regions are observed in the vicinity of the point $\{x = 0$ cm, $y = -1.7$

*In MARS and FLUKA calculations the right-handed coordinate system is used, *i.e.*, X-axis is up, Y-axis is to the right, and Z-axis is along the beam.

cm} in the TCDS (see Fig. 3) and approximately in the middle of the 6-mm septa in the MSD-1 (see Fig. 2).

Comparisons between the peak distributions calculated with the FLUKA and MARS codes are presented in Figs. 5 and 6. The observed difference in temperature rise (Fig. 5) to some extent is due to different temperature dependences of specific heat, $C(T)$, used in the two codes. To eliminate the systematic difference, calculated peak energy deposition densities are compared in Fig. 6 for baseline luminosity (straightforward scaling is applicable for energy deposition at ultimate luminosity). The observed agreement between the two codes is quite reasonable.

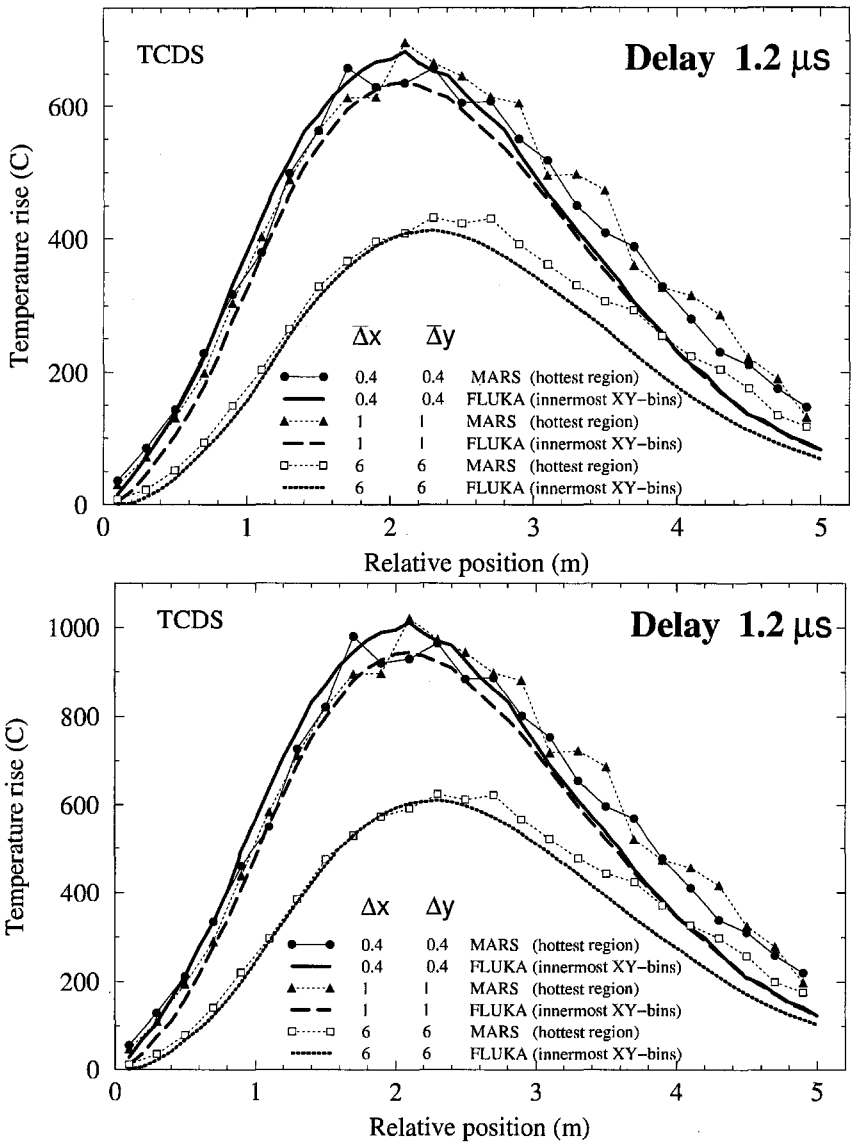

Figure 5: Temperature rise distribution in the TCDS collimator at baseline (top) and ultimate (bottom) luminosities. Δx and Δy are in *mm*.

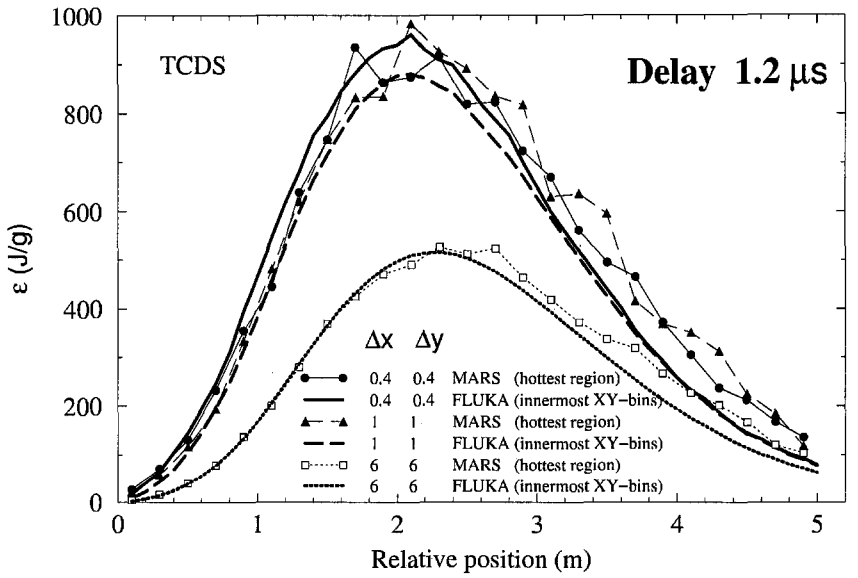

Figure 6: Energy deposition density distributions in the TCDS collimator at baseline luminosity. Δx and Δy are in *mm*.

The instantaneous peak temperature rises for the baseline and ultimate beam intensities are given in Table 3. They refer to the maxima over the cells $1\times6\times100$, $1\times1\times100$, and $0.5\times11\times500$ mm^3 for the TCDS, MSD-1, and TCDQ, respectively. The observed deviation from linear scaling with the beam intensity is due to temperature dependence of the specific heat, $C(T)$. Statistical uncertainties (hereinafter 1σ) are equal to 5% for TCDS and TCDQ-1 and 10% for MSD-1 and TCDQ-2.

Table 3: Instantaneous peak temperature rise ΔT (C) in the collimators and the first of the IP6 MSD modules at baseline (1.05×10^{11} ppb)) (left) and ultimate (1.7×10^{11} ppb) (right) beam intensity.

Module	Delay time τ (μs)		
	1.2	3.0	4.0
TCDS	698	680	694
MSD-1	522	450	504
TCDQ-1 (4 m)	456	810	1170
TCDQ-2 (4 m)	155	246	348
TCDQ-3 (1.5 m)	5	14	34

Module	Delay time τ (μs)		
	1.2	3.0	4.0
TCDS	1018	993	1015
MSD-1	785	653	715
TCDQ-1 (4 m)	651	1167	1697
TCDQ-2 (4 m)	227	355	499
TCDQ-3 (1.5 m)	9	23	55

A single pre-fired kicker is not strong enough to deflect the beam significantly for it to hit the TCDS collimator. Deflected bunches hit the collimator when the other fired kickers attain a given strength. That is why almost no dependence of

instantaneous peak temperature rise in the TCDS collimator and MSD modules on delay time is observed in the results presented. One can conclude that the TCDS and TCDQ collimators can safely survive an unsynchronized beam abort. The rather high local temperature in the MSD-1 magnet is a concern and will be addressed by optimizing the TCDS collimator, with the use of a more dense downstream section if necessary.

6 Energy Deposition in SC Magnets

The peak energy deposition density ε_{max} was calculated for the SC coils from Q4 up to MBB-2. These values should be compared to the quench limit that can be estimated as 0.5 mJ/g per pulse for the LHC magnets at fast beam loss ($\leq$20 μs) [6]. The calculated values of ε_{max} in the seven SC magnets considered, along with the statistical uncertainties, are presented in Fig. 7, with the word "peak" referring to the highest value over length of each magnet. One can conclude that no SC coils in the LHC will be damaged at an unsynchronized abort for the delay times considered (energy deposition as high as a few hundred of J/g is required to melt down a metal). The first seven to ten SC magnets downstream of IP6 will, however, be subject to quench. When comparing to the previous results [2], the peak values for Q4 and Q5 quads are almost the same, while for the subsequent downstream magnets some changes are observed. It should be noted, however, that the present calculated statistical uncertainty for these magnets was almost three times as low as previously, so that the present results are more reliable.

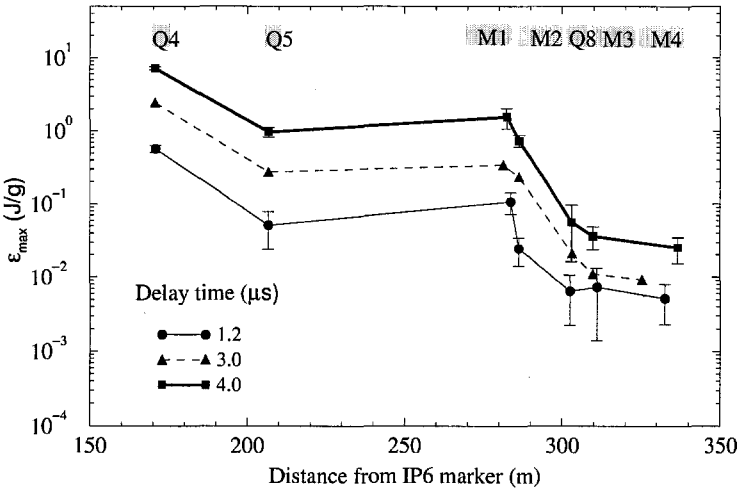

Figure 7: Distribution of peak energy deposition density ε_{max} in SC magnets *vs.* distance from IP6, where M1 - M4 denote the first four dipoles in the region (see Table 2).

7 Radiation Levels in Tunnel

An unsynchronized beam abort gives rise to instantaneous irradiation in the tunnel. Distributions of equivalent dose can be useful to estimate dose load during such an accident and determine the most dangerous regions. The distributions have been calculated in the tunnel in the vicinity of the vessel and near the farthest concrete wall and are shown in Fig. 8. One can conclude from the results that the most dangerous regions are near the collimators TCDS and TCDQ. Almost no dependence of equivalent dose in the vicinity of the TCDS collimator on delay time is observed because the number of bunches which hit the collimator do not depend on delay time (see section 5). On the contrary, in the region of the TCDQ collimator the equivalent dose increases with delay time. The increase is more significant at a distance behind the collimator, *e.g.* near Q4, than in its immediate vicinity (one order of magnitude and a factor of two, respectively).

The calculations have been performed assuming that there is no contribution to dose in tunnel in the vicinity of IP6 due to the extracted beam which is supposed to be directed to an external beam dump.

8 Conclusions

The proposed protection system will reliably protect the machine components from an unsynchronized abort in the LHC IP6. No beam losses in the IP5 are found with the proposed collimators TCDS and TCDQ in the appropriate position. The study revealed that, with this system, the peak temperature rise in most of the IP6 components is quite acceptable. The rather high local temperature in the MSD-1 magnet will need some further optimization of the TCDS design. All the LHC SC dipoles and quadrupoles are protected against damage in the event of such an accident. At the same time, the first seven to ten SC magnets after IP6 are subject to quench at unsynchronized abort, even for the lowest delay time considered (1.2 μs). To complete this study, further work is required to take into account final design of the MSD vacuum chamber and final position of the magnets and collimators TCDS and TCDQ.

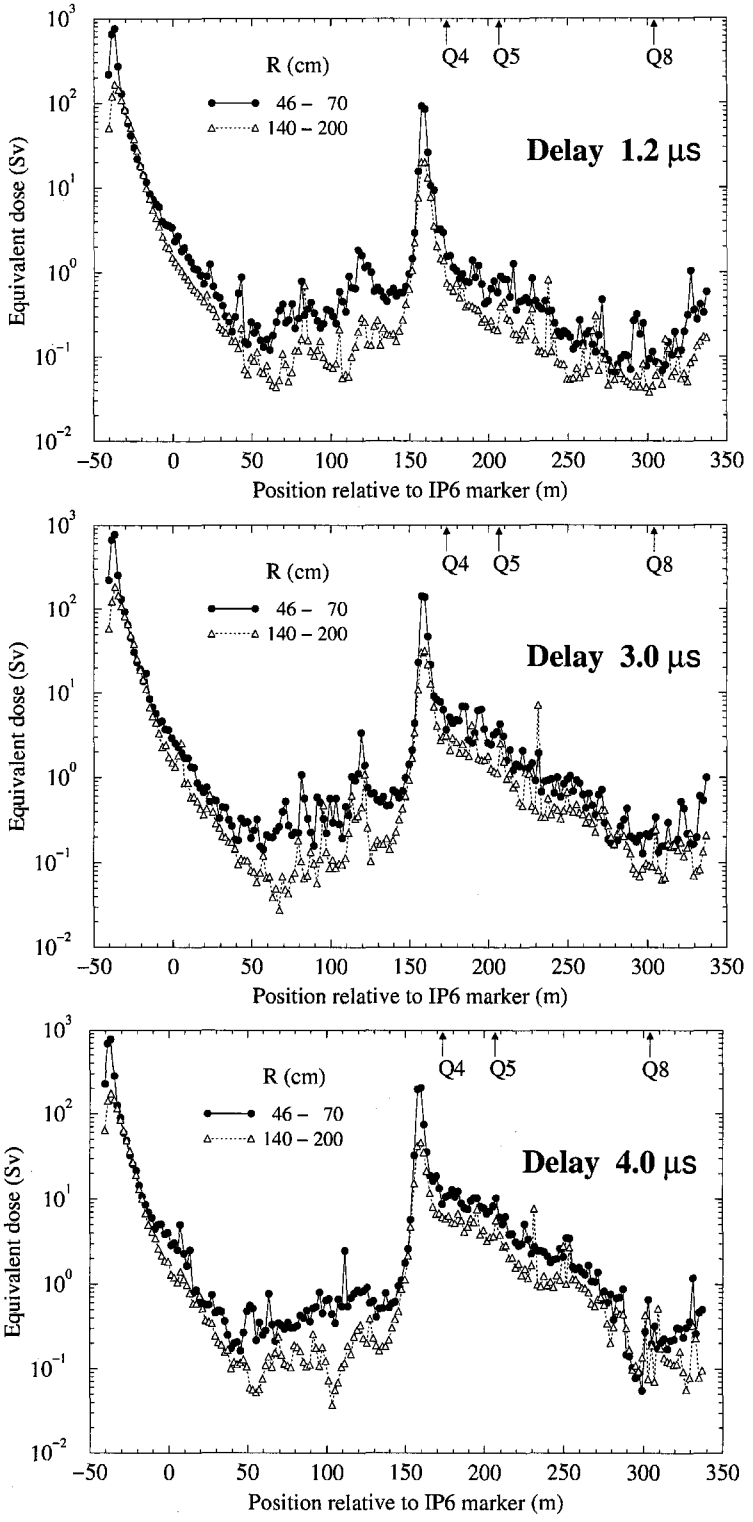

Figure 8: Distribution of instantaneous equivalent dose in tunnel in the vicinity of the vessel (46-70 cm) and near the farthest concrete wall (140-200 cm) due to the unsynchronized beam abort at different delay times.

References

[1] A.I. Drozhdin, N.V. Mokhov, M. Huhtinen, Proc. of the 1999 Part. Accel. Conf., New York, 1999, p. 1231; Fermilab-Conf-99/060 (1999).

[2] N.V. Mokhov, A.I. Drozhdin, I.L. Rakhno, M. Gyr, E. Weisse, "Protecting LHC components against radiation resulting from an unsynchronized beam abort", Fermilab-Conf-01/133 (2001); LHC Project Report 478, CERN, Geneva (2001); Part. Accel. Conf., Chicago, 2001, p. 3168.

[3] N.V. Mokhov, "The MARS Code System User's Guide", Fermilab-FN-628 (1995); N.V. Mokhov and O.E. Krivosheev, "MARS Code Status", Fermilab-Conf-00/181 (2000). http://www-ap.fnal.gov/MARS/.

[4] A. Fassø, A. Ferrari, J. Ranft, P.R. Sala, "New developments in FLUKA modelling hadronic and EM interactions", *Proc. 3rd Workshop on Simulating Accelerator Radiation Environments*, KEK, Tsukuba, Japan, 7-9 May 1997, Ed. H. Hirayama, KEK Proceedings 97-5, p. 32-43 (1997); A. Ferrari, and P.R. Sala, "The Physics of High Energy Reactions", *Proc. the Workshop on Nuclear Reaction Data and Nuclear Reactors Physics, Design and Safety*, International Centre for Theoretical Physics, Miramare-Trieste, Italy, 15 April-17 May 1996, edited by A. Gandini and G. Reffo, World Scientific, p. 424 (1998).

[5] N. V. Mokhov, "Energy Deposition in Targets and Beam Dumps at 0.1-5 TeV Proton Energy", Fermilab-FN-328 (1980); A. N. Kalinovsky, N. V. Mokhov, and Yu. P. Nikitin, "Passage of High-Energy Particles through Matter", AIP, New York (1989).

[6] Fermilab Superconducting Accelerator Design Report, Fermilab, 1979.